
Modeling dynamic social vision highlights gaps between deep learning and humans

Kathy Garcia^{1*} Emalie McMahon^{1*} Colin Conwell¹ Michael F. Bonner¹ Leyla Isik^{1,2}

*authors contributed equally

¹Department of Cognitive Science, Johns Hopkins University

²Department of Biomedical Engineering, Johns Hopkins University

{kgarci18, emaliemcmahon, cconwell12, mfbonner, lisik}@jhu.edu

Abstract

Deep learning models trained on computer vision tasks are widely considered the most successful models of human vision to date. The majority of work that supports this idea evaluates how accurately these models predict brain and behavioral responses to static images of objects and natural scenes. Real-world vision, however, is highly dynamic, and far less work has focused on evaluating the accuracy of deep learning models in predicting responses to stimuli that move, and that involve more complicated, higher-order phenomena like social interactions. Here, we present a dataset of natural videos and captions involving complex multi-agent interactions, and we benchmark 350+ image, video, and language models on behavioral and neural responses to the videos. As with prior work, we find that many vision models reach the noise ceiling in predicting visual scene features and responses along the ventral visual stream (often considered the primary neural substrate of object and scene recognition). In contrast, image models poorly predict human action and social interaction ratings and neural responses in the lateral stream (a neural pathway increasingly theorized as specializing in dynamic, social vision). Language models (given human sentence captions of the videos) predict action and social ratings better than either image or video models, but they still perform poorly at predicting neural responses in the lateral stream. Together these results identify a major gap in AI's ability to match human social vision and highlight the importance of studying vision in dynamic, natural contexts.

1 Introduction

Over the past decade, significant advances have been made in understanding the computations underlying both biological and artificial vision, in large part due to deep learning models that now provide the best match to human visual behavior and neural responses. However, most research has focused exclusively on static scene and object recognition, neglecting the rich, dynamic interactions that characterize real-world vision. Human vision is particularly tuned to process dynamic social scenes from an early age [1], yet social vision remains a substantial open challenge in artificial intelligence (AI) [2]. Current AI models struggle to match even human infants in their ability to understand social scenes [3, 4]. Many have argued that incorporating insights from cognitive (neuro)science may improve AI models' performance on social tasks [5, 6, 7]. However, AI vision and language models are rapidly evolving, and current models have never been comprehensively tested against humans in dynamic, social vision.

The human brain processes dynamic social scenes in regions that are distinct from those involved in classical object perception [8, 9, 6, 10]. These regions form the recently proposed lateral visual stream [11, 12], specialized for dynamic social perception and distinct from the classical ventral “what” and dorsal “where” streams [13, 14]. While AI models effectively predict the ventral stream’s computations, little is known about the lateral stream’s computations. Recent work suggests computational similarities between the ventral and lateral streams, proposing that lateral stream representations may also be hierarchical, with each computational stage yielding increasingly abstract representations [15]. Some work has even suggested that lateral stream computations are not distinct from ventral stream computations [16, 17]. However, this claim is based on visually-evoked responses to static images, while lateral stream regions respond minimally—if at all—to static stimuli [18, 19].

Here, we use a large-scale benchmarking approach to investigate the computational principles of human social perception and identify areas of critical need for AI model development (Figure 1). Using over 350 image, video, and language models, we predict human behavioral ratings and fMRI responses to a dataset of publicly-available natural videos depicting human social actions [15]. We find that language models based on sentence captions of the videos are best at predicting human social ratings and that video models are best, on average, at predicting brain responses in the lateral visual stream. However, the performance in lateral stream regions is substantially lower than performance in the ventral visual stream, and no model is able to match both human behavior and brain data. Together, these results highlight a critical need for image-computable models of social perception that match human abilities.

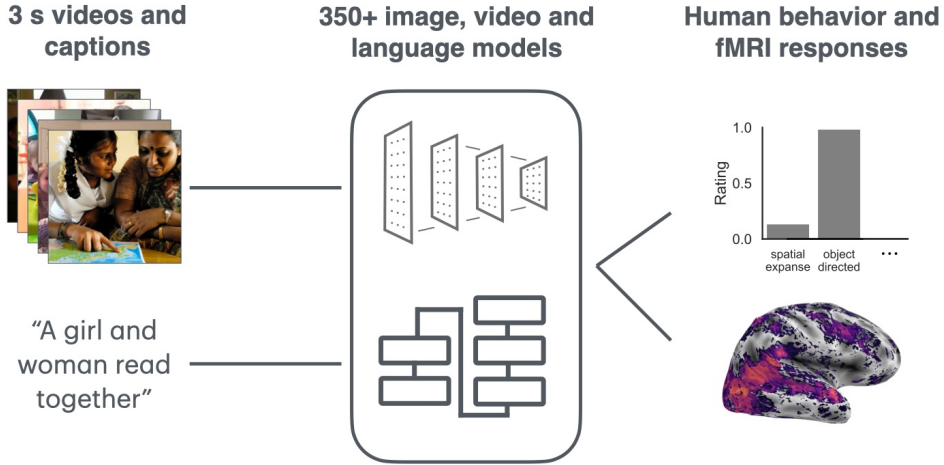


Figure 1: A summary of our overall approach. We extract representations from over 350 image, video, and language models based on 3 s videos of human social actions or their captions. We then use model representations to predict human behavioral ratings and the neural responses recorded using fMRI to the videos.

2 Related Work

Our approach builds on the NeuroAI benchmarking approach that has been popularized by others [20, 21, 22, 23, 24, 25, 26]. NeuroAI benchmarking often aims to identify either the single best model of the brain or behavior [20, 21, 22, 23] or to understand the computational principles underlying human-model alignment [24, 25, 26]. Here, we take the latter approach, but rather than aiming to understand static scene responses in the ventral visual stream, which are well modeled by most current image models [24], we aim to understand dynamic visual responses across the brain, focusing on the lateral visual stream. In addition to benchmarking vision models, we also use language models to predict behavioral ratings and visually-evoked neural responses as has been done in prior work with static scenes [27, 28, 29, 30, 31, 32]. As in Conwell et al. [27], we use multiple language models as predictors and selectively perturb the sentence captions of the stimuli to provide insights into the kind of linguistic features that are predictive of visual responses. While modeling dynamic visual

events is a growing area of interest [32], this is the first investigation of benchmarking many models in response to naturalistic videos of human actions.

3 Methods

3.1 Code and data availability

All code used in this paper and our sentence captions are publicly available: (*redacted for anonymity, see supplemental files*). The social action ratings and fMRI responses from the original dataset [15] are publicly available on OSF <https://osf.io/4j29y/> with a CC-By Attribution 4.0 International license. The videos shown to participants and used here to extract model activations are from the Moments in Time (MiT) dataset <http://moments.csail.mit.edu>. The MiT license restricts public release of videos from the dataset, but the videos are provided with the paper for review and instructions to obtain the videos are available with the original dataset.

3.2 Social action dataset

Here, we model behavioral ratings and neural responses from a publicly available dataset of human social actions [15]. The dataset includes 250 three-second videos of social actions that are divided into 200 videos for training alignment models and 50 videos for evaluation.

Each video includes human behavioral ratings of the visual and social scene. The rated dimensions include descriptions of the visual scene such as how large the scene is (spatial expanse); physical relations between people such as how close together they are (interagent distance) and the extent to which they are facing one another (agents facing); the extent to which an action is object-directed (object directed); social descriptions including the extent to which people are jointly engaged in an action (acting jointly), the extent to which they are communicating (communicating) and affective features (valence and arousal). Ratings were collected on a Likert scale by at least ten subjects, and we use the average rating for each feature.

The dataset also includes fMRI neural responses to each of the videos in four participants, and an estimate of the explainable variance determined as the test-retest reliability of responses to the same videos. The fMRI data also includes anatomically (early visual cortex, EVC, and motion-selective middle temporal area, MT) and functionally-defined regions of interest (ROIs) in the ventral and lateral streams. The ventral functional ROIs include the face-selective fusiform face area (FFA) [33] and place-selective parahippocampal place area (PPA) [34], and the lateral ROIs include the extrastriate body area (EBA), which processes bodies and relations between bodies [35, 36], the lateral occipital cortex (LOC) which is object selective [37] and is involved in processing object-directed actions [38], and posterior and anterior social-interaction selective regions in the STS (pSTS and aSTS) [38, 39, 10, 15].

3.3 Sentence captioning of videos

In order to evaluate language model prediction of behavioral and neural responses, we collected sentence captions of the videos from 150 online participants using the Prolific platform, and in accordance with our Institutional Review Board. Eligibility criteria included having completed at least 50 tasks with an 85% approval rate, having normal vision (or corrected-to-normal), and being native English speakers. Participants were compensated approximately \$12 per hour on average for their participation.

Following informed consent, each participant captioned 12 videos presented in a random order: 10 videos from the dataset used in McMahon et al. [15] and 2 additional catch videos. Each video appeared with a text box with grayed out text that read “Description of the actions and interactions of the people in the video in a single sentence...” and disappeared when the subject began typing their caption. We collected at least five unique captions for each video. Captions were cleaned by removing participants whose captions on either of the catch videos was more than 2.5 standard deviations away from the mean of other participants in the embedding space of Hugging Face’s fine-tuned all-MiniLM-L12-v1 [40, 41]. All-MiniLM-L12-v1 was not reused in subsequent analyses.

3.4 DNN model selection

We selected models with a broad range of architectures, training sets and objectives. In total, we tested 342 image models from collections including Torchvision [42] and Pytorch-Image-Models libraries [43], VISSL [44], OpenAI CLIP [45], and Detectron2 [46]. We selected eight video models. Notable video models included Facebook’s SlowFast [47] and TimeSformer [48] models. Image and video models were selected to represent a comprehensive cross-section of high-level visual tasks, and include convolutional and transformer architectures. Fifteen language models were selected, focusing on sentence-transformers, including GPT-2 [49] and BERT variants [50]. For full model list, please see the supplemental files. We tested fewer video and language models relative to image models due to their availability and computational requirements, respectively. However, this only strengthens our conclusions when either model class outperforms image models.

3.5 Model alignment with behavioral and neural responses

3.5.1 Model feature extraction

We utilized DeepJuice [24], a python package in alpha-release shared with us by the authors, that allows for memory efficient feature extraction from each layer of a DNN. We extracted the intermediate representations from every unique computational submodule (referred to here as layers) of every model. We then used GPU-optimized sparse random projection (SRP) implemented in the python package to project the activations in an approximately 4732-dimensional feature space based on the Johnson–Lindenstrauss lemma with $\epsilon = 0.1$ [51].

All model inputs were preprocessed in a model-specific manner. For image models, we extracted activations for seven evenly-sampled frames across the three-seconds of each video and then averaged the activations across frames from the same video. In preliminary analyses, we found that this produced almost identical results to using activations from only a single frame or concatenating activations across the seven-frames. Similar to image models, for language models, we extracted the activations for each caption, and then averaged the activations for the captions from the same video.

3.5.2 Linear mapping

Before fitting the linear mapping, we first z-scored the model-SRP feature space across the samples independently for each feature in the 200-video train set defined in the original dataset [15] and then normalized the held-out data from 50 videos by the mean and standard deviation from the train set. We normalized the behavioral and neural data using the same procedure.

We performed linear mapping between the normalized model-SRP feature space and the normalized behavioral or neural response using leave-one-out ridge regression optimized for the GPU as implemented in DeepJuice [24]. Our α -penalty search space was seven values sampled from a logspace of $10e^{-2}, 10e^5$. In the training set, we performed 4-fold cross validation in a full sweep of the model to determine the layer that produced the highest performance on the held-out data. Performance was measured as the Pearson correlation between the predicted behavioral or neural response and the true response.

We selected the optimal model layer based on this cross-validation in the training set, and evaluated each models’ performance for the optimal layer in the test set. The optimal model layer was selected separately for every behavioral rating and voxel in the brain. For the brain data, we only predicted responses in voxels that were determined to have high test-retest reliability in the original dataset.

3.6 Caption perturbation experiment

To gain insight into what aspect of the captions produced high alignment between the language models and the brain/behavior, we performed selective perturbations to the captions as in [27, 52], but instead of deletion, we performed masking to keep the overall syntactic structure of the sentence intact. We used the spaCy [53] package and the en_core_web_sm model in particular to identify the parts of speech for masking. All other aspects of the experiment followed our model-brain/behavior mapping procedure described above.

3.7 Statistical analysis

To determine whether there was a difference in mean performance between classes of models (e.g., image relative to language), we first computed a null distribution for each model by correlating the permuted predicted response and actual response over 5000 iterations. The same shuffling procedure was used across all models. We compared the true mean difference between model classes to a null distribution of mean differences. The p-value was determined by performing a two-tailed test of the true value against the permuted distributions.

The same procedure was used to determine whether a perturbation on the sentence captions significantly decreased alignment between the language models and the brain/behavior, except using a one-tailed test to compare true degradation (performance on the “original” minus performance on perturbed sentence) to chance.

3.8 Compute specifications

The ridge regression for the encoding models required a substantial amount of computational resources. We used an institutional high performance computing cluster equipped with 31 A100 GPU nodes (with a mix of 40 and 80 GB memory). On average, each set of model regressions took approximately 0.38 core hours for the whole-brain results and 0.39 core hours for behavior rating results, for a total of 0.77 core hours per model. To run the full suite of 365 image, video and language models for the reported results took approximately 280 core hours. Full computational resources for the research project (including failed experiments and experiments not reported here) required approximately 1600 core hours.

4 Results

4.1 Behavioral ratings

4.1.1 Language models capture human visual social ratings better than vision models

In evaluating the models, we can compare both how the different model classes (image, video, or language) perform on average at predicting each caption (Figure 2) and the top performing model for each rating (Supplemental Table 1). We note that due to the larger number of image models tested, the best performing model is biased towards the image models. Despite this, we see a large amount of similarity between the two metrics.

We find that for the visuospatial ratings (spatial expanse, interagent distance, and agents facing), no model class is substantially better on average ($p > 0.05$), but for each rating the top performing model is an image model. In contrast, for all social and action ratings, the best performing model is a language model despite the over-representation of image models in our model set. For predicting ratings of object directed actions and communicating, the mean difference between language and vision models is not significant ($p > 0.05$). For ratings of agents acting jointly and affective features (valence and arousal), language models perform better on average than image models ($ps < 0.01$) and video models ($ps < 0.001$), except for valence ($p < 0.05$).

For most ratings, video models do not perform better than image models, except for predictions of communicating, valence, and arousal ($ps < 0.05$). Within the image models, we do not see different predictions for models with a convolutional versus transformer architecture (Supplemental Figure 8) or based on a supervised versus self-supervised learning objective (Supplemental Figure 7). Together, these results suggest that drastically different visual models perform similarly in predicting video ratings.

4.1.2 Human-Language Model alignment depends on both noun and verb content

To understand the features driving high language model predictivity, we performed selective perturbations on sentence captions by removing nouns or verbs from the captions (Figure 3A). We calculate the degradation in performance as the score of the original, unperturbed input captions (r_o) minus the score of the perturbed input captions (r_p) divided by the score of the original (r_o).

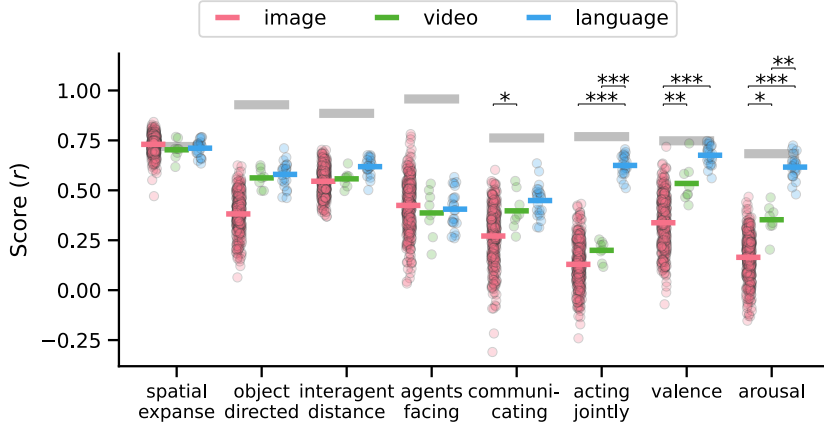


Figure 2: Prediction performance of all models in predicting behavioral responses. Each dot is the performance of a single model. The lines indicate the mean performance for image (pink), video (green), and language (blue) models. The horizontal gray lines are the inter-subject agreement, which is approximately the maximal level that any model could be expected to perform. Brackets and asterisks indicate significantly different performance between different classes of models ($p < 0.05$: *, $p < 0.01$: **, $p < 0.001$: ***).

We find that when predicting most ratings shuffling the input captions does not decrease performance, except spatial expanse and agents acting jointly ($p < 0.05$), suggesting that behavior-model alignment does not rely on linguistic compositional structure (Figure 3B).

We can group the remaining perturbations based on disruption to noun content (no nouns, only verbs, teals in Figure 3B) and disruptions to verb content (no verbs, only nouns, pinks in Figure 3B). Prediction of most ratings is degraded by disrupting noun content ($ps < 0.05$), except for agents facing and communicating. Prediction of most ratings is also degraded by both verb manipulations (no verbs and only nouns, $ps < 0.05$), except ratings of object directed actions ($p > 0.05$) and interagent distance ($ps > 0.05$). Together, these results suggest that the success of language models in predicting visual responses relies on both noun and verb content, with the exception of agents facing / communication and object-directedness, respectively.

4.2 Neural responses

4.2.1 Vision models best capture neural responses

As in behavior, we can compare both the average performance of the models, and the best model for each ROI (Supplemental Table 2). We evaluate performance in ROIs (Figure 4) and the whole brain (Figure 5). We find that for several mid-level ROIs (MT, EBA, and LOC), video models dramatically outperform image models ($ps < 0.001$). In both early visual cortex and high-level lateral regions (pSTS and aSTS), the quantitative performance gain is moderate and not significantly different ($ps > 0.05$), and the best performing model is an image model. Within the image models, we do not find a notable difference in performance for models with either convolutional or transformer architectures (Supplemental Figure 10) or trained through supervised or self-supervision objectives (Supplemental Figure 11), further underscoring the importance of video processing as a critical manipulation within video models.

Contrary to what we see in behavior, language models do not outperform vision models on average in any region ($ps > 0.05$), but they dramatically underperform in EVC, FFA, and PPA ($ps < 0.01$), and there is no ROI in which the best model is a language model. Language perturbation experiments suggest both noun and verb content are important for prediction in most ROIs (Figure 12).

Despite the relatively higher performance by video models in predicting responses in the lateral regions, we still see a striking under performance of even the best model relative to ventral regions.

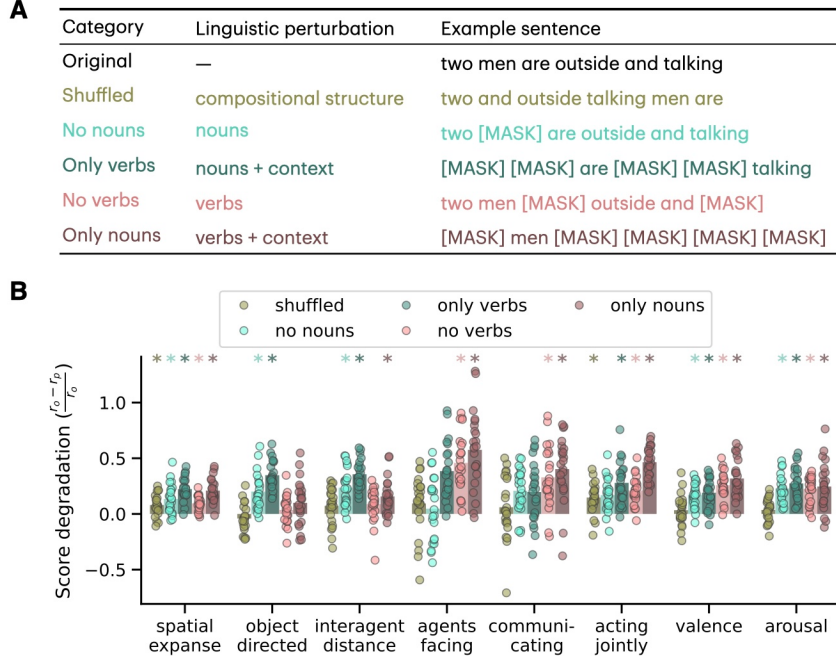


Figure 3: **A.** Example sentence perturbations. **B.** The performance of each language model (dots) in predicting human behavioral ratings following selective perturbation of the sentence captions. The bars indicate the mean performance across models for each condition and rating. Asterisks indicate that there is a significant degradation in model-behavioral alignment following perturbation relative to the unperturbed sentence.

4.2.2 Hierarchical alignment between models and brains

Previous investigations have found a hierarchical correspondence between vision models and the brain in the ventral temporal cortex in humans [54] and inferiortemporal cortex in macaques [55, 56]. We investigated whether there was a similar hierarchical correspondence between models and responses in lateral visual regions by evaluating the relative depth of each voxel in the whole brain (Figure 6) and on average in our regions of interest (Figure 9). We find that though early visual cortex is best predicted by earlier layers in the models, all other regions are predicted by layers of approximately equal depth. In contrast, whole brain results do reveal a hierarchy along the ventral stream, thus highlighting an additional gap between models and neural representations in the lateral visual stream.

5 Discussion

We use a large-set of image, video, and language models to predict human behavioral ratings and neural responses to dynamic social scenes. Overall, we found a notable gap in all models’ ability to predict human responses. However, there are differences in the models that are best able to predict the brain versus behavior. In particular, language models tend to be the best models of human behavioral ratings, while videos models best predict responses in lateral brain regions.

5.1 Language and video models for social scene understanding

The fact that language models align with human social ratings may suggest that humans rely on non-visual aspects of social interactions to rate social features [15, 57]. While this may be partially true, it is unlikely to be the whole answer because humans make many of these social judgements quickly and automatically [6, 58]. Further, these behavioral ratings strongly predict visual regions of the brain [15, 6], which the language models cannot explain. Another reason the language models predict behavior so well may be due to the captioning prompt. By instructing participants to caption the “actions and interactions” in the videos, we might have biased the language model embeddings to

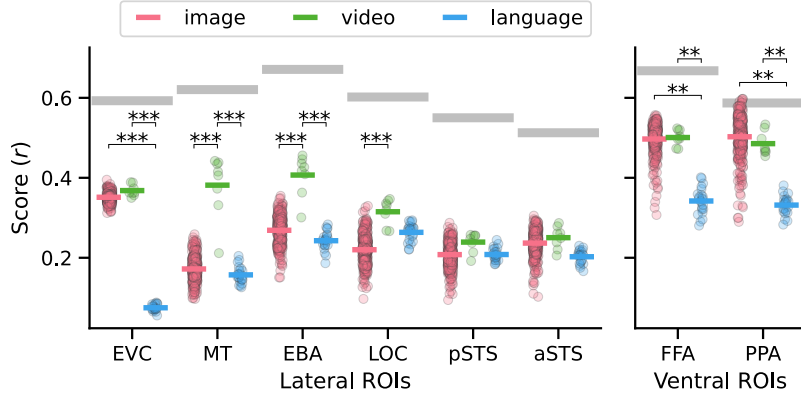


Figure 4: The performance of each model (dots) in predicting the average response in each ROI. The colored lines indicate the mean performance of the different classes of models, and the horizontal gray line is the split-half reliability of the voxel responses in each ROI averaged across participants. Brackets and asterisks indicate significantly different performance between different classes of models ($p < 0.05$: *, $p < 0.01$: **, $p < 0.001$: ***).

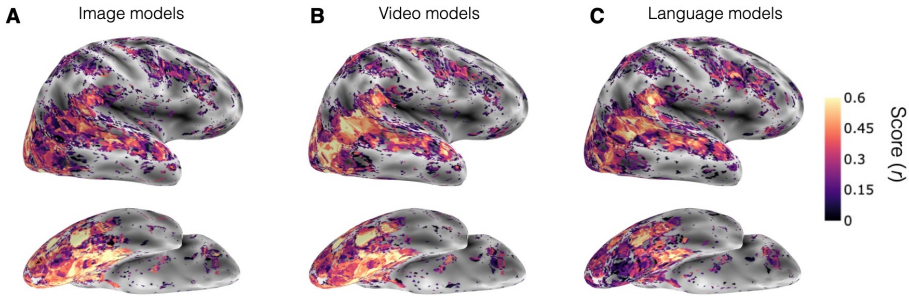


Figure 5: Visualization of the test set encoding performance of the best performing layer in the training set for each voxel from any (A) image, (B) video, and (C) language model. This is shown on the lateral and ventral surface in right hemisphere of one representative participant.

better predict social action content. It is therefore somewhat surprising that language models do not perform better because, for example, high-communication videos are often captioned explicitly with verbs like “talking” (e.g., example caption in Figure 3), and yet most language models still fall short of human agreement.

In contrast, video models provided a surprising boost to prediction in mid-level lateral regions, which is striking given the lack of available high-performing video models relative to image models, but they did not predict behavioral ratings or more anterior regions significantly better than image models. Together, this work reveals a significant gap in even state-of-the-art models abilities to match human social action judgements and the underlying neural substrates. These results also provide insights into future directions for model development that can integrate both the relational structure that is readily present in language with dynamic visual information.

5.2 NeuroAI in dynamic social contexts

One major advantage of this work over most prior NeuroAI studies is the focus on dynamic, social scenes. In addition to the human-model gap described above, several other interesting findings come out of testing models in more ecologically valid conditions. First, prior work has suggested that

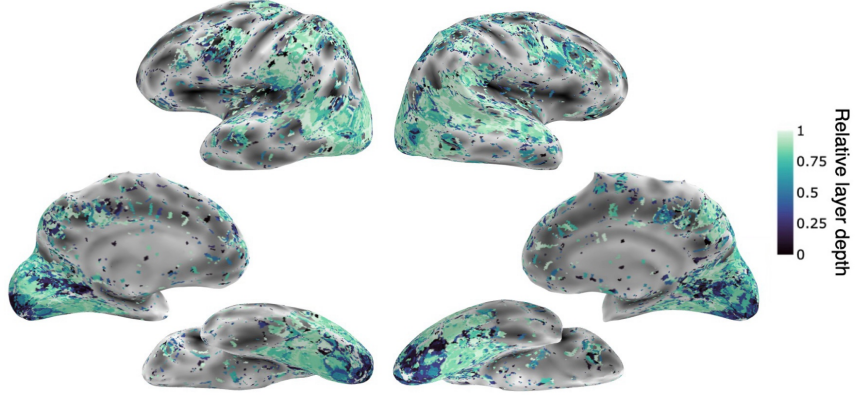


Figure 6: Relative depth of the best performing model layer across all vision models (image and video models) in the whole brain of one representative subject.

affective features like valence and arousal can be extracted by relatively simple convolutional neural networks [59, 60]. While these features may be image computable, our work shows that in dynamic events, few existing vision models can match human social-affective ratings.

Further, unlike prior work with static scenes [27, 28], language models are not able to capture brain responses in the current dataset. They perform dramatically worse than image models in predicting responses in EVC as has been documented elsewhere [27] but also significantly worse in high-level ventral regions (Figures 4, 5). This result calls into question strong ideas of “language alignment” in visual cortex and highlights the importance of dynamic stimuli for studies of even the ventral visual stream [61].

5.3 Limitations

More work is needed both in cognitive (neuro)science and computer science to gain insights into the computations underlying human social perception. One plausible direction in both domains is the collection of larger, more varied video datasets. A limitation of the current study is that the human dataset we modeled here only contained behavioral and neural responses to 250 naturalistic video clips. While larger dynamic neuroscience datasets do exist [32], they are not yet publicly available and do not rival existing static image datasets [62]. Likewise, computer vision video datasets [63, 64, 65] lack the size and diversity of image datasets [66, 65].

Another major limitation of this benchmarking approach is that it takes advantage of available models that differ along many factors, making it difficult to isolate the role of any one computational factor. This limitation may explain why we do not see significant differences for seemingly important model factors, like convolutional versus transformer architectures (Supplemental Figures 8, 10), for example. We aimed to overcome this by testing a wide array of models, but as noted above, our set includes relatively few video and language models compared to image models. Future work should investigate how larger language models compare to human on social visual tasks, though we note here that the largest language model tested (GPT-2) was far from the top performing model in most tests (Supplemental Tables 1, 2).

5.4 Conclusions

This work identifies human social vision as a key area of need for future AI research. It also offers some promising directions for future modeling endeavors. In particular, the relative success of language and video models over image models in predicting social behavior and brain responses suggests that models combining both compositional and dynamic information may be critical for more human-like social AI.

References

- [1] J. Kiley Hamlin, Karen Wynn, and Paul Bloom. Social evaluation by preverbal infants. *Nature*, 450(7169):557–559, November 2007. ISSN 1476-4687. doi: 10.1038/nature06288. URL <https://doi.org/10.1038/nature06288>.
- [2] Samuele Bolotta and Guillaume Dumas. Social Neuro AI: Social Interaction as the “Dark Matter” of AI. *Frontiers in Computer Science*, 4, 2022. ISSN 2624-9898. URL <https://www.frontiersin.org/articles/10.3389/fcomp.2022.846440>.
- [3] Kanishk Gandhi, Gala Stojnic, Brenden M. Lake, and Moira R. Dillon. Baby Intuitions Benchmark (BIB): Discerning the goals, preferences, and actions of others, February 2022. URL <http://arxiv.org/abs/2102.11938>; arXiv:2102.11938 [cs].
- [4] Tianmin Shu, Abhishek Bhandwaldar, Chuang Gan, Kevin Smith, Shari Liu, Dan Gutfreund, Elizabeth Spelke, Joshua Tenenbaum, and Tomer Ullman. AGENT: A Benchmark for Core Psychological Reasoning. In *Proceedings of the 38th International Conference on Machine Learning*, pages 9614–9625. PMLR, July 2021. URL <https://proceedings.mlr.press/v139/shu21a.html>. ISSN: 2640-3498.
- [5] Chen Zhou, Ming Han, Qi Liang, Yi-Fei Hu, and Shu-Guang Kuai. A social interaction field model accurately identifies static and dynamic social groupings. *Nature Human Behaviour*, 3(8):847–855, August 2019. ISSN 2397-3374. doi: 10.1038/s41562-019-0618-2. URL <https://www.nature.com/articles/s41562-019-0618-2>; Publisher: Nature Publishing Group.
- [6] Emalie McMahon and Leyla Isik. Seeing social interactions. *Trends in Cognitive Sciences*, 27(12):1165–1179, December 2023. ISSN 13646613. doi: 10.1016/j.tics.2023.09.001. URL <https://linkinghub.elsevier.com/retrieve/pii/S1364661323002486>.
- [7] Manasi Malik and Leyla Isik. Relational visual representations underlie human social interaction recognition. *Nature Communications*, 14(1):7317, November 2023. ISSN 2041-1723. doi: 10.1038/s41467-023-43156-8. URL <https://www.nature.com/articles/s41467-023-43156-8>; Number: 1 Publisher: Nature Publishing Group.
- [8] Leyla Tarhan and Talia Konkle. Sociality and interaction envelope organize visual action representations. *Nature Communications*, 11(1):3002, June 2020. ISSN 2041-1723. doi: 10.1038/s41467-020-16846-w. URL <https://www.nature.com/articles/s41467-020-16846-w>.
- [9] Moritz F. Wurm, Alfonso Caramazza, and Angelika Lingnau. Action Categories in Lateral Occipitotemporal Cortex Are Organized Along Sociality and Transitivity. *Journal of Neuroscience*, 37(3):562–575, 2017. ISSN 0270-6474. doi: 10.1523/JNEUROSCI.1717-16.2016. URL <https://www.jneurosci.org/content/37/3/562>; Publisher: Society for Neuroscience _eprint: <https://www.jneurosci.org/content/37/3/562.full.pdf>.
- [10] Haemy Lee Masson and Leyla Isik. Functional selectivity for social interaction perception in the human superior temporal sulcus during natural viewing. *NeuroImage*, 245:118741, December 2021. ISSN 10538119. doi: 10.1016/j.neuroimage.2021.118741. URL <https://linkinghub.elsevier.com/retrieve/pii/S1053811921010132>.
- [11] David Pitcher and Leslie G. Ungerleider. Evidence for a Third Visual Pathway Specialized for Social Perception. *Trends in Cognitive Sciences*, 25(2):100–110, February 2021. ISSN 13646613. doi: 10.1016/j.tics.2020.11.006. URL <https://linkinghub.elsevier.com/retrieve/pii/S1364661320302783>.
- [12] Moritz F. Wurm and Alfonso Caramazza. Two ‘what’ pathways for action and object recognition. *Trends in Cognitive Sciences*, 26(2):103–116, February 2022. ISSN 13646613. doi: 10.1016/j.tics.2021.10.003. URL <https://linkinghub.elsevier.com/retrieve/pii/S1364661321002588>.
- [13] Leslie G. Ungerleider and Mortimer Mishkin. Two cortical visual systems. In David J. Ingle, Melvyn A. Goodale, and Richard J. W. Mansfield, editors, *Analysis of Visual Behavior*, pages 549–586. The MIT Press, 1982.

- [14] Melvyn A. Goodale and A. David Milner. Separate visual pathways for perception and action. *Trends in Neurosciences*, 15(1):20–25, 1992. ISSN 0166-2236. doi: [https://doi.org/10.1016/0166-2236\(92\)90344-8](https://doi.org/10.1016/0166-2236(92)90344-8). URL <https://www.sciencedirect.com/science/article/pii/0166223692903448>.
- [15] Emalie McMahon, Michael F. Bonner, and Leyla Isik. Hierarchical organization of social action features along the lateral visual pathway. preprint, PsyArXiv, March 2023. URL <https://osf.io/x3avb>
- [16] Dawn Finzi, Daniel Yamins, Kendrick Kay, and Kalanit Grill-Spector. Do deep convolutional neural networks accurately model representations beyond the ventral stream? In 2022 Conference on Cognitive Computational Neuroscience, San Francisco, 2022. Cognitive Computational Neuroscience. doi: 10.32470/CCN.2022.1219-0. URL https://2022.ccneuro.org/view_paper.php?PaperNum=1219.
- [17] Dawn Finzi, Eshed Margalit, Kendrick Kay, Daniel L. K. Yamins, and Kalanit Grill-Spector. A single computational objective drives specialization of streams in visual cortex, December 2023. URL <https://www.biorxiv.org/content/10.1101/2023.12.19.572460v1>. Pages: 2023.12.19.572460 Section: New Results.
- [18] Emmanuelle Bellot, Etienne Abassi, and Liuba Papeo. Moving Toward versus Away from Another: How Body Motion Direction Changes the Representation of Bodies and Actions in the Visual Cortex. *Cerebral Cortex*, 31(5):2670–2685, January 2021. ISSN 1047-3211. doi: 10.1093/cercor/bhaa382. URL <https://doi.org/10.1093/cercor/bhaa382> _eprint: <https://academic.oup.com/cercor/article-pdf/31/5/2670/36840949/bhaa382.pdf>.
- [19] Julia Landsiedel, Katie Daughters, Paul E. Downing, and Kami Koldewyn. The role of motion in the neural representation of social interactions in the posterior temporal cortex. *NeuroImage*, 262:119533, November 2022. ISSN 1053-8119. doi: 10.1016/j.neuroimage.2022.119533. URL <https://www.sciencedirect.com/science/article/pii/S1053811922006486>
- [20] Martin Schrimpf, Jonas Kubilius, Ha Hong, Najib J. Majaj, Rishi Rajalingham, Elias B. Issa, Kohitij Kar, Pouya Bashivan, Jonathan Prescott-Roy, Franziska Geiger, Kailyn Schmidt, Daniel L. K. Yamins, and James J. DiCarlo. Brain-Score: Which Artificial Neural Network for Object Recognition is most Brain-Like? preprint, Neuroscience, September 2018. URL <http://biorxiv.org/lookup/doi/10.1101/407007>.
- [21] Martin Schrimpf, Jonas Kubilius, Michael J Lee, N Apurva Ratan Murty, Robert Ajemian, and James J DiCarlo. Integrative benchmarking to advance neurally mechanistic models of human intelligence. *Neuron*, 2020. URL [https://www.cell.com/neuron/fulltext/S0896-6273\(20\)30605-X](https://www.cell.com/neuron/fulltext/S0896-6273(20)30605-X)
- [22] A. T. Gifford, B. Lahner, S. Saba-Sadiya, M. G. Vilas, A. Lascelles, A. Oliva, K. Kay, G. Roig, and R. M. Cichy. The Algonauts Project 2023 Challenge: How the Human Brain Makes Sense of Natural Scenes, July 2023. URL <http://arxiv.org/abs/2301.03198>. arXiv:2301.03198 [cs, q-bio].
- [23] Konstantin F. Willeke, Paul G. Fahey, Mohammad Bashiri, Laura Pede, Max F. Burg, Christoph Blessing, Santiago A. Cadena, Zhiwei Ding, Konstantin-Klemens Lurz, Kayla Ponder, Taliah Muhammad, Saumil S. Patel, Alexander S. Ecker, Andreas S. Tolias, and Fabian H. Sinz. The Sensorium competition on predicting large-scale mouse primary visual cortex activity, June 2022. URL <http://arxiv.org/abs/2206.08666>. arXiv:2206.08666 [cs, q-bio].
- [24] Colin Conwell, Jacob S. Prince, Kendrick N. Kay, George A. Alvarez, and Talia Konkle. What can 1.8 billion regressions tell us about the pressures shaping high-level visual representation in brains and machines?, July 2023. URL <https://www.biorxiv.org/content/10.1101/2022.03.28.485868v2>. Pages: 2022.03.28.485868 Section: New Results.
- [25] Eric Elmoznino and Michael F. Bonner. High-performing neural network models of visual cortex benefit from high latent dimensionality. *PLOS Computational Biology*, 20(1):e1011792, January 2024. ISSN 1553-7358. doi: 10.1371/journal.pcbi.1011792. URL <https://journals.plos.org/ploscompbiol/article?id=10.1371/journal.pcbi.1011792>. Publisher: Public Library of Science.

- [26] Zirui Chen and Michael Bonner. Canonical dimensions of vision. In *2023 Conference on Cognitive Computational Neuroscience*, Oxford, UK, 2023. Cognitive Computational Neuroscience. doi: 10.32470/CCN.2023.1588-0. URL https://2023.ccneuro.org/view_paper.php?PaperNum=1588.
- [27] Colin Conwell, Jacob S. Prince, George A. Alvarez, and Talia Konkle. Language Models of Visual Cortex: Where do they work? And why do they work so well where they do? *Journal of Vision*, 23(9):5653, August 2023. ISSN 1534-7362. doi: 10.1167/jov.23.9.5653. URL <https://jov.arvojournals.org/article.aspx?articleid=2792615>.
- [28] Adrien Doerig, Tim C. Kietzmann, Emily Allen, Yihan Wu, Thomas Naselaris, Kendrick Kay, and Ian Charest. Semantic scene descriptions as an objective of human vision, September 2022. URL <http://arxiv.org/abs/2209.11737>, arXiv:2209.11737 [cs, q-bio].
- [29] Robert Geirhos, Kantharaju Narayananappa, Benjamin Mitzkus, Tizian Thieringer, Matthias Bethge, Felix A. Wichmann, and Wieland Brendel. Partial success in closing the gap between human and machine vision, October 2021. URL <http://arxiv.org/abs/2106.07411>, arXiv:2106.07411 [cs, q-bio].
- [30] Drew Linsley, Ivan F. Rodriguez Rodriguez, Thomas Fel, Michael Arcaro, Saloni Sharma, Margaret Livingstone, and Thomas Serre. Performance-optimized deep neural networks are evolving into worse models of inferotemporal visual cortex. *Advances in Neural Information Processing Systems*, 36:28873–28891, December 2023. URL https://proceedings.neurips.cc/paper_files/paper/2023/hash/5bf234ecf83cd77bc5b77a24ba9338b0-Abstract-Conference.html.
- [31] Thomas Fel, Ivan F Rodriguez Rodriguez, Drew Linsley, and Thomas Serre. Harmonizing the object recognition strategies of deep neural networks with humans. In S. Koyejo, S. Mohamed, A. Agarwal, D. Belgrave, K. Cho, and A. Oh, editors, *Advances in Neural Information Processing Systems*, volume 35, pages 9432–9446. Curran Associates, Inc., 2022. URL https://proceedings.neurips.cc/paper_files/paper/2022/file/3d681cc4487b97c08e5aa67224dd74f2-Paper-Conference.pdf.
- [32] Benjamin Lahner, Kshitij Dwivedi, Polina Iamshchinina, Monika Graumann, Alex Lascelles, Gemma Roig, Alessandro Thomas Gifford, Bowen Pan, Sou Young Jin, N. Apurva Ratan Murty, Kendrick Kay, Aude Oliva, and Radoslaw Cichy. BOLD Moments: modeling short visual events through a video fMRI dataset and metadata, March 2023. URL <https://www.biorxiv.org/content/10.1101/2023.03.12.530887v1>, Pages: 2023.03.12.530887 Section: New Results.
- [33] Nancy Kanwisher, Josh McDermott, and Marvin M. Chun. The Fusiform Face Area: A Module in Human Extrastriate Cortex Specialized for Face Perception. *The Journal of Neuroscience*, 17(11):4302–4311, June 1997. ISSN 0270-6474, 1529-2401. doi: 10.1523/JNEUROSCI.17-11-04302.1997. URL <https://www.jneurosci.org/lookup/doi/10.1523/JNEUROSCI.17-11-04302.1997>
- [34] Russell Epstein and Nancy Kanwisher. A cortical representation of the local visual environment. *Nature*, 392(6676):598–601, April 1998. ISSN 0028-0836, 1476-4687. doi: 10.1038/33402. URL <https://www.nature.com/articles/33402>.
- [35] Paul E. Downing, Yuhong Jiang, Miles Shuman, and Nancy Kanwisher. A Cortical Area Selective for Visual Processing of the Human Body. *Science*, 293(5539):2470–2473, 2001. doi: 10.1126/science.1063414. Publisher: American Association for the Advancement of Science.
- [36] Etienne Abassi and Liuba Papeo. The Representation of Two-Body Shapes in the Human Visual Cortex. *Journal of Neuroscience*, 40(4):852–863, 2020. doi: 10.1523/JNEUROSCI.1378-19.2019. Publisher: Society for Neuroscience.
- [37] Kalanit Grill-Spector, Zoe Kourtzi, and Nancy Kanwisher. The lateral occipital complex and its role in object recognition. *Vision Research*, 41(10-11):1409–1422, May 2001. ISSN 00426989. doi: 10.1016/S0042-6989(01)00073-6. URL <https://linkinghub.elsevier.com/retrieve/pii/S0042698901000736>

- [38] Leyla Isik, Kami Koldewyn, David Beeler, and Nancy Kanwisher. Perceiving social interactions in the posterior superior temporal sulcus. *Proceedings of the National Academy of Sciences*, 114(43), October 2017. ISSN 0027-8424, 1091-6490. doi: 10.1073/pnas.1714471114. URL <https://pnas.org/doi/full/10.1073/pnas.1714471114>.
- [39] Jon Walbrin, Paul Downing, and Kami Koldewyn. Neural responses to visually observed social interactions. *Neuropsychologia*, 112:31–39, April 2018. ISSN 1873-3514. doi: 10.1016/j.neuropsychologia.2018.02.023.
- [40] Thomas Wolf, Lysandre Debut, Victor Sanh, Julien Chaumond, Clement Delangue, Anthony Moi, Pierrick Cistac, Tim Rault, Rémi Louf, Morgan Funtowicz, Joe Davison, Sam Shleifer, Patrick von Platen, Clara Ma, Yacine Jernite, Julien Plu, Canwen Xu, Teven Le Scao, Sylvain Gugger, Mariama Drame, Quentin Lhoest, and Alexander M. Rush. HuggingFace’s Transformers: State-of-the-art Natural Language Processing, July 2020. URL <http://arxiv.org/abs/1910.03771>. arXiv:1910.03771 [cs].
- [41] Wenhui Wang, Furu Wei, Li Dong, Hangbo Bao, Nan Yang, and Ming Zhou. MiniLM: Deep Self-Attention Distillation for Task-Agnostic Compression of Pre-Trained Transformers, April 2020. URL <http://arxiv.org/abs/2002.10957>. arXiv:2002.10957 [cs].
- [42] TorchVision maintainers and contributors. Torchvision: Pytorch’s computer vision library. <https://github.com/pytorch/vision>, 2016.
- [43] Ross Wightman. Pytorch image models. <https://github.com/rwightman/pytorch-image-models>, 2019.
- [44] Priya Goyal, Quentin Duval, Jeremy Reizenstein, Matthew Leavitt, Min Xu, Benjamin Lefauveux, Mannat Singh, Vinicius Reis, Mathilde Caron, Piotr Bojanowski, Armand Joulin, and Ishan Misra. ViSSL. <https://github.com/facebookresearch/vissl>, 2021.
- [45] Alec Radford, Jong Wook Kim, Chris Hallacy, Aditya Ramesh, Gabriel Goh, Sandhini Agarwal, Girish Sastry, Amanda Askell, Pamela Mishkin, Jack Clark, Gretchen Krueger, and Ilya Sutskever. Learning Transferable Visual Models From Natural Language Supervision, February 2021. URL <http://arxiv.org/abs/2103.00020>. arXiv:2103.00020 [cs].
- [46] Yuxin Wu, Alexander Kirillov, Francisco Massa, Wan-Yen Lo, and Ross Girshick. Detectron2. <https://github.com/facebookresearch/detectron2>, 2019.
- [47] Christoph Feichtenhofer, Haoqi Fan, Jitendra Malik, and Kaiming He. SlowFast Networks for Video Recognition. *arXiv*: 1812.03982, 2018.
- [48] Gedas Bertasius, Heng Wang, and Lorenzo Torresani. Is Space-Time Attention All You Need for Video Understanding?, June 2021. URL <http://arxiv.org/abs/2102.05095>. arXiv:2102.05095 [cs].
- [49] Alec Radford, Jeff Wu, Rewon Child, David Luan, Dario Amodei, and Ilya Sutskever. Language models are unsupervised multitask learners. 2019.
- [50] Jacob Devlin, Ming-Wei Chang, Kenton Lee, and Kristina Toutanova. BERT: Pre-training of Deep Bidirectional Transformers for Language Understanding, May 2019. URL <http://arxiv.org/abs/1810.04805>. arXiv:1810.04805 [cs].
- [51] Kasper Green Larsen and Jelani Nelson. The Johnson-Lindenstrauss lemma is optimal for linear dimensionality reduction, November 2014. URL <http://arxiv.org/abs/1411.2404>. arXiv:1411.2404 [cs, math].
- [52] Carina Kauf, Greta Tuckute, Roger Levy, Jacob Andreas, and Evelina Fedorenko. Lexical-Semantic Content, Not Syntactic Structure, Is the Main Contributor to ANN-Brain Similarity of fMRI Responses in the Language Network. *Neurobiology of Language*, 5(1):7–42, April 2024. ISSN 2641-4368. doi: 10.1162/nol_a_00116. URL https://doi.org/10.1162/nol_a_00116.
- [53] Matthew Honnibal and Ines Montani. spaCy 2: Natural language understanding with Bloom embeddings, convolutional neural networks and incremental parsing. To appear, 2017.

- [54] Kalanit Grill-Spector and Kevin S. Weiner. The functional architecture of the ventral temporal cortex and its role in categorization. *Nature Reviews Neuroscience*, 15(8):536–548, 2014. doi: 10.1038/nrn3747. URL <https://www.ncbi.nlm.nih.gov/pmc/articles/PMC4143420/>.
- [55] Daniel L. K. Yamins, Ha Hong, Charles F. Cadieu, Ethan A. Solomon, Darren Seibert, and James J. DiCarlo. Performance-optimized hierarchical models predict neural responses in higher visual cortex. *Proceedings of the National Academy of Sciences*, 111(23):8619–8624, June 2014. ISSN 0027-8424, 1091-6490. doi: 10.1073/pnas.1403112111. URL <https://pnas.org/doi/full/10.1073/pnas.1403112111>.
- [56] Seyed-Mahdi Khaligh-Razavi and Nikolaus Kriegeskorte. Deep Supervised, but Not Unsupervised, Models May Explain IT Cortical Representation. *PLoS Computational Biology*, 10(11):e1003915, November 2014. ISSN 1553-7358. doi: 10.1371/journal.pcbi.1003915. URL <https://dx.plos.org/10.1371/journal.pcbi.1003915>.
- [57] Aviv Netanyahu, Tianmin Shu, Boris Katz, Andrei Barbu, and Joshua B. Tenenbaum. PHASE: PHysically-grounded Abstract Social Events for Machine Social Perception, March 2021. URL <http://arxiv.org/abs/2103.01933>, arXiv:2103.01933 [cs, stat].
- [58] Susanne Quadflieg and Ian S. Penton-Voak. The Emerging Science of People-Watching: Forming Impressions From Third-Party Encounters. *Current Directions in Psychological Science*, 26(4):383–389, August 2017. ISSN 0963-7214. doi: 10.1177/0963721417694353. URL <https://doi.org/10.1177/0963721417694353>. Publisher: SAGE Publications Inc.
- [59] Philip A. Kragel, Marianne C. Reddan, Kevin S. LaBar, and Tor D. Wager. Emotion schemas are embedded in the human visual system. *Science Advances*, 5(7):eaaw4358, July 2019. doi: 10.1126/sciadv.aaw4358. URL <https://www.science.org/doi/10.1126/sciadv.aaw4358>. Publisher: American Association for the Advancement of Science.
- [60] Colin Conwell, Daniel Graham, and Edward A Vessel. The perceptual primacy of feeling: Affectless machine vision models robustly predict human visual arousal, valence, and aesthetics. 2021.
- [61] James V. Haxby, M. Ida Gobbini, and Samuel A. Nastase. Naturalistic stimuli reveal a dominant role for agentic action in visual representation. *NeuroImage*, 216:116561, August 2020. ISSN 1095-9572. doi: 10.1016/j.neuroimage.2020.116561.
- [62] Emily J. Allen, Ghislain St-Yves, Yihan Wu, Jesse L. Breedlove, Jacob S. Prince, Logan T. Dowdle, Matthias Nau, Brad Caron, Franco Pestilli, Ian Charest, J. Benjamin Hutchinson, Thomas Naselaris, and Kendrick Kay. A massive 7T fMRI dataset to bridge cognitive neuroscience and artificial intelligence. *Nature Neuroscience*, 25(1):116–126, January 2022. ISSN 1097-6256, 1546-1726. doi: 10.1038/s41593-021-00962-x. URL <https://www.nature.com/articles/s41593-021-00962-x>.
- [63] Will Kay, Joao Carreira, Karen Simonyan, Brian Zhang, Chloe Hillier, Sudheendra Vijayanarasimhan, Fabio Viola, Tim Green, Trevor Back, Paul Natsev, Mustafa Suleyman, and Andrew Zisserman. The Kinetics Human Action Video Dataset. *arXiv: 1705.06950*, 2017.
- [64] Mathew Monfort, Alex Andonian, Bolei Zhou, Kandan Ramakrishnan, Sarah Adel Bargal, Tom Yan, Lisa Brown, Quanfu Fan, Dan Gutfruend, Carl Vondrick, and others. Moments in Time Dataset: one million videos for event understanding. *IEEE Transactions on Pattern Analysis and Machine Intelligence*, pages 1–8, 2019. ISSN 0162-8828. doi: 10.1109/TPAMI.2019.2901464.
- [65] Bart Thomee, David A. Shamma, Gerald Friedland, Benjamin Elizalde, Karl Ni, Douglas Poland, Damian Borth, and Li-Jia Li. YFCC100M: The New Data in Multimedia Research. *Communications of the ACM*, 59(2):64–73, January 2016. ISSN 0001-0782, 1557-7317. doi: 10.1145/2812802. URL <http://arxiv.org/abs/1503.01817>, arXiv:1503.01817 [cs].
- [66] J. Deng, W. Dong, R. Socher, L. Li, Kai Li, and Li Fei-Fei. ImageNet: A large-scale hierarchical image database. In *2009 IEEE Conference on Computer Vision and Pattern Recognition*, pages 248–255, 2009. doi: 10.1109/CVPR.2009.5206848.

A Supplemental materials

Table 1: A table of the top-30 performing models averaged across features. Models are arranged in descending order of their overall average performance. Bold scores highlight the model that is the top performing model for a given feature.

Rank	Model name	Model class	spatial expanse	object directed	inter-agent distance	agents facing	communicating	acting jointly	valence	arousal
1	paraphrase-MiniLM-L6-v2	language	0.764	0.576	0.664	0.524	0.635	0.583	0.692	0.684
2	all-mppnet-base-v2	language	0.688	0.665	0.676	0.537	0.384	0.678	0.743	0.725
3	paraphrase-multilingual-MiniLM-L12-v2	language	0.725	0.609	0.621	0.523	0.595	0.625	0.684	0.647
4	all-mppnet-base-v1	language	0.766	0.711	0.615	0.424	0.313	0.643	0.747	0.709
5	FacebookAI_roberta-large-mnli	language	0.725	0.605	0.608	0.567	0.468	0.683	0.664	0.605
6	mixedbread-ai_mxba1-embed-2d-large-v1	language	0.766	0.520	0.670	0.541	0.431	0.706	0.686	0.588
7	paraphrase-multilingual-mppnet-base-v2	language	0.735	0.610	0.652	0.462	0.504	0.660	0.705	0.572
8	all-distilroberta-v1	language	0.722	0.582	0.605	0.458	0.465	0.603	0.709	0.638
9	stsbs-distilroberta-base-v2	language	0.660	0.624	0.623	0.401	0.506	0.586	0.720	0.621
10	all-roberta-large-v1	language	0.760	0.548	0.621	0.428	0.400	0.691	0.634	0.613
11	distiluse-base-miltilingual-cased-v1	language	0.740	0.630	0.669	0.266	0.489	0.582	0.656	0.651
12	clip-ViT-B-32-multilingual-v1	language	0.709	0.607	0.545	0.399	0.483	0.669	0.724	0.541
13	clip_vitl14	image	0.771	0.535	0.660	0.781	0.492	0.319	0.718	0.392
14	mixedbread-ai_mxba1-colbert-large-v1	language	0.660	0.540	0.570	0.432	0.528	0.670	0.652	0.599
15	mixedbread-ai_mxba1-embed-large-v1	language	0.690	0.558	0.633	0.465	0.461	0.630	0.631	0.570
16	all-MiniLM-L6-v2	language	0.700	0.627	0.579	0.343	0.481	0.529	0.661	0.636
17	FacebookAI_xlm-roberta-large	language	0.729	0.650	0.602	0.357	0.401	0.620	0.561	0.612
18	all-MiniLM-L6-v1	language	0.634	0.605	0.676	0.260	0.492	0.611	0.596	0.637
19	FacebookAI_xlm-roberta-base	language	0.657	0.494	0.641	0.357	0.374	0.610	0.732	0.633
20	multi-qa-MiniLM-L6-cos-v1	language	0.686	0.461	0.648	0.337	0.347	0.643	0.668	0.700
21	gpt2	language	0.730	0.599	0.637	0.340	0.315	0.555	0.624	0.631
22	LaBSE	language	0.648	0.550	0.563	0.274	0.477	0.674	0.625	0.568
23	timm_deit3_large_patch16_224_in21ft1k	image	0.820	0.504	0.663	0.628	0.371	0.340	0.629	0.300
24	FacebookAI_roberta-base	language	0.727	0.499	0.607	0.335	0.400	0.511	0.696	0.480
25	all-MiniLM-L12-v2	language	0.731	0.465	0.501	0.288	0.373	0.603	0.733	0.515
26	timm_beit2_large_patch16_224	image	0.842	0.503	0.642	0.667	0.505	0.358	0.417	0.143
27	timm_deit3_base_patch16_224_in21ft1k	image	0.789	0.498	0.584	0.649	0.291	0.375	0.514	0.333
28	timm_beit_large_patch16_224	image	0.828	0.506	0.703	0.755	0.277	0.184	0.588	0.184
29	timm_beit_large_patch16_384	image	0.811	0.565	0.644	0.705	0.278	0.298	0.634	0.084
30	timm_deit3_large_patch16_384_in21ft1k	image	0.804	0.510	0.617	0.597	0.481	0.417	0.333	0.224

Table 2: A table of the top-30 models on averaged across all ROIs. Models are arranged in descending order of their overall average performance in all reliable voxels. Bold scores highlight the top score in each ROI.

Rank	Model name	Model class	EVC	MT	EBA	LOC	pSTS	aSTS	FFA	PPA
1	x3d_s	video	0.389	0.442	0.427	0.347	0.256	0.261	0.519	0.521
2	timm_beitv2_base_patch16_224	image	0.369	0.245	0.349	0.326	0.275	0.293	0.536	0.588
3	timm_beitv2_large_patch16_224	image	0.376	0.259	0.355	0.330	0.287	0.291	0.524	0.593
4	x3d_m	video	0.388	0.435	0.456	0.343	0.247	0.287	0.516	0.493
5	timm_beit_large_patch16_224	image	0.373	0.241	0.335	0.314	0.277	0.297	0.520	0.592
6	timm_beit_large_patch16_384	image	0.368	0.251	0.336	0.317	0.253	0.266	0.501	0.593
7	clip_vitl14	image	0.376	0.223	0.325	0.289	0.245	0.278	0.526	0.574
8	timm_deit3_huge_patch14_224_in21ft1k	image	0.375	0.233	0.320	0.291	0.264	0.287	0.538	0.587
9	timm_deit3_large_patch16_384_in21ft1k	image	0.376	0.241	0.328	0.292	0.253	0.276	0.517	0.574
10	timm_beit_base_patch16_224	image	0.365	0.228	0.322	0.298	0.258	0.267	0.522	0.578
11	timm_deit3_large_patch16_224_in21ft1k	image	0.372	0.241	0.337	0.295	0.245	0.274	0.499	0.584
12	timm_convnext_large_in22ft1k	image	0.373	0.230	0.318	0.284	0.252	0.273	0.502	0.559
13	timm_convnext_large	image	0.373	0.230	0.318	0.284	0.252	0.273	0.502	0.559
14	timm_convnext_xlarge_in22k	image	0.370	0.219	0.303	0.283	0.256	0.265	0.515	0.555
15	i3d_r50	video	0.361	0.416	0.446	0.336	0.255	0.262	0.493	0.450
16	timm_deit3_medium_patch16_224_in21ft1k	image	0.363	0.228	0.348	0.284	0.249	0.270	0.522	0.568
17	c2d_r50	video	0.374	0.373	0.409	0.310	0.257	0.279	0.515	0.460
18	timm_convnext_xlarge_in22ft1k	image	0.372	0.233	0.320	0.285	0.247	0.268	0.501	0.558
19	slow_r50	video	0.356	0.406	0.418	0.319	0.237	0.221	0.492	0.465
20	clip_rn50x4	image	0.376	0.229	0.316	0.277	0.237	0.272	0.552	0.568
21	timm_convnext_large_in22k	image	0.368	0.225	0.307	0.269	0.249	0.282	0.520	0.555
22	timm_beit_base_patch16_384	image	0.358	0.230	0.331	0.292	0.235	0.266	0.512	0.568
23	timm_convnext_base	image	0.364	0.225	0.324	0.275	0.240	0.258	0.517	0.549
24	timm_convnext_base_in22ft1k	image	0.364	0.225	0.324	0.275	0.240	0.258	0.517	0.549
25	timm_deit3_base_patch16_224_in21ft1k	image	0.362	0.217	0.321	0.286	0.224	0.257	0.539	0.576
26	timm_mixer_b16_224_miil_in21k	image	0.395	0.219	0.304	0.253	0.234	0.290	0.541	0.555
27	clip_vitb32	image	0.376	0.203	0.300	0.246	0.262	0.241	0.507	0.568
28	timm_deit3_base_patch16_384_in21ft1k	image	0.367	0.209	0.289	0.269	0.248	0.269	0.526	0.566
29	timm_convnext_base_in22k	image	0.362	0.217	0.308	0.276	0.228	0.250	0.515	0.559
30	timm_mixer_b16_224_miil	image	0.384	0.218	0.311	0.268	0.232	0.290	0.543	0.568

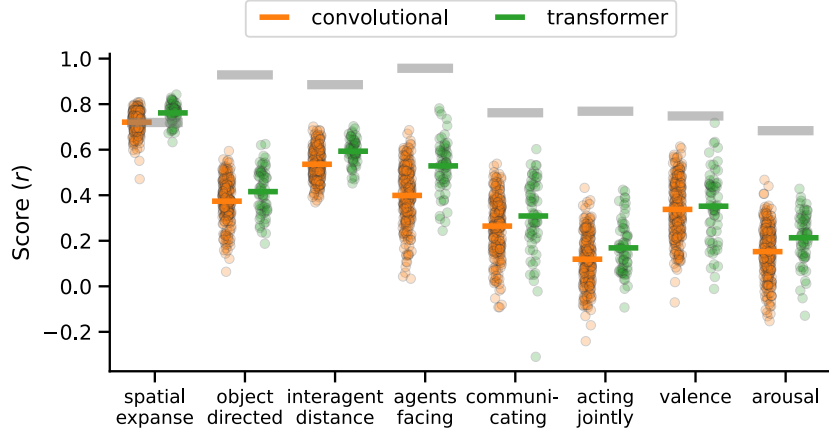


Figure 7: The performance of each image model in our set in predicting behavioral responses separated by whether the model has a convolutional (orange) or transformer (green) architecture. Plotting conventions are the same as Figure 2

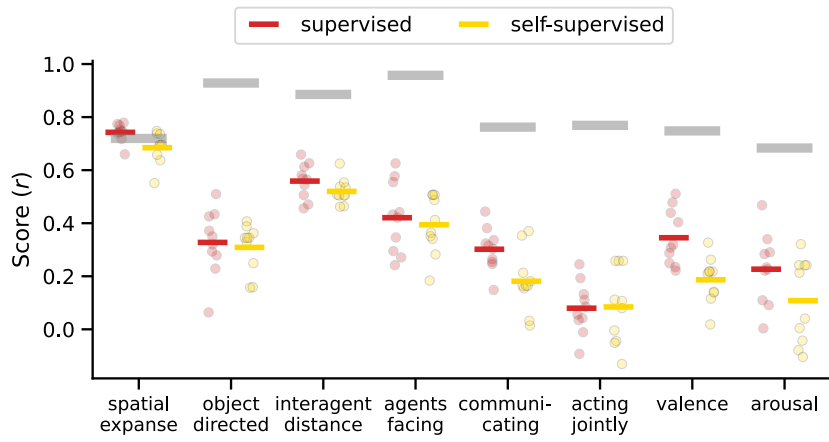


Figure 8: The performance of each image model in our set with a ResNet-50 backbone in predicting behavioral responses separated by whether the model uses a supervised (red) or self-supervised (yellow) learning objective. This analysis was restricted to a single architecture class (ResNet-50) to focus specifically on the learning objective. Plotting conventions are the same as Figure 2

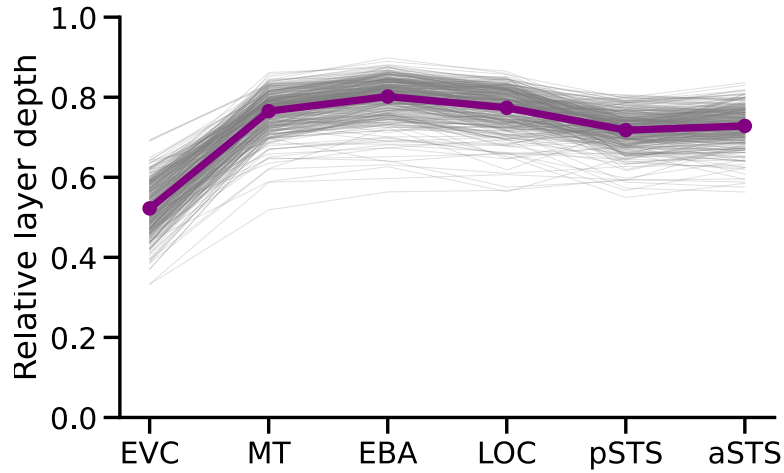


Figure 9: The relative layer depth of the best performing model layer for each image and video model (thin gray lines) and the average best layer depth across models (thick purple line) in each ROI along the lateral visual stream.

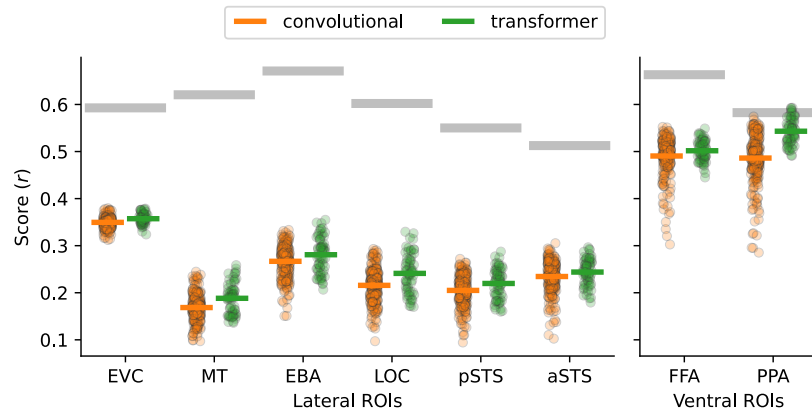


Figure 10: The performance of each image model in our set in predicting neural responses in ROIs in the lateral and ventral visual streams. Models are grouped by convolutional (orange) or transformer (green) architecture. Plotting conventions are the same as Figure 4.

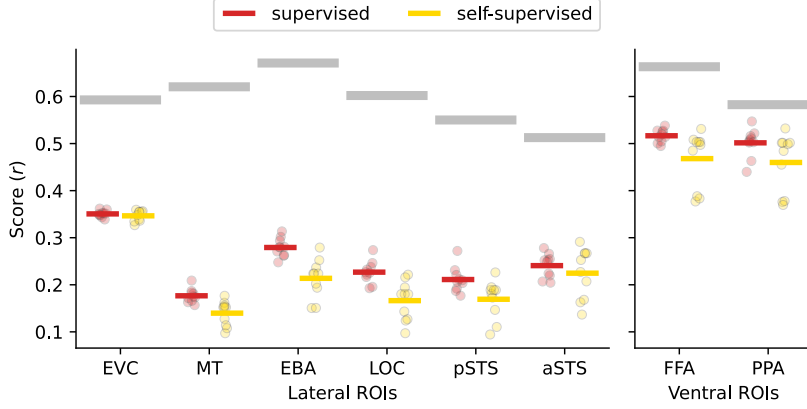


Figure 11: The performance by each image models with a ResNet-50 backbone in predicting neural responses in ROIs in the lateral and ventral visual streams. Models are grouped by supervised (red) or self-supervised (green) learning objective. This analysis was restricted to a single architecture class (ResNet-50) to focus specifically on the training objective. Plotting conventions are the same as Figure 4.

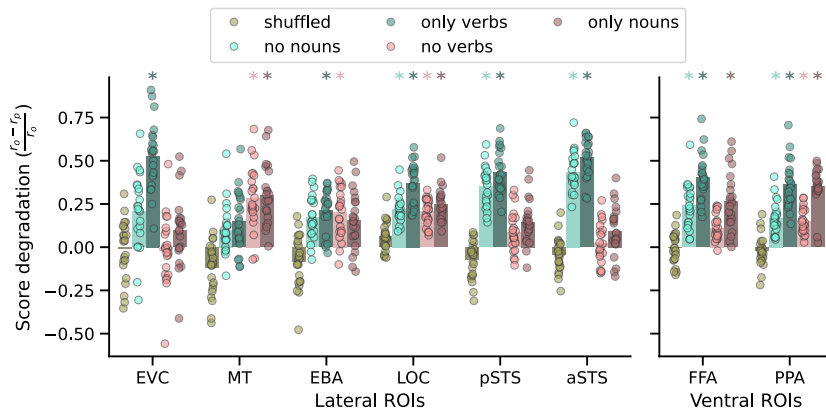


Figure 12: The average performance in ROIs of each language model (dots) in predicting neural responses following selective perturbation of the sentence captions. The bars indicate the mean performance across models for each condition and rating. Asterisks indicate that there is a significant degradation in model-neural alignment following perturbation relative to the unperturbed sentence.